



# HP1 $\beta$ carries an acidic linker domain and requires H3K9me3 for phase separation

Weihua Qin, Andreas Stengl, Enes Ugur, Susanne Leidescher, Joel Ryan, M. Cristina Cardoso & Heinrich Leonhardt

To cite this article: Weihua Qin, Andreas Stengl, Enes Ugur, Susanne Leidescher, Joel Ryan, M. Cristina Cardoso & Heinrich Leonhardt (2021) HP1 $\beta$  carries an acidic linker domain and requires H3K9me3 for phase separation, Nucleus, 12:1, 44-57, DOI: [10.1080/19491034.2021.1889858](https://doi.org/10.1080/19491034.2021.1889858)

To link to this article: <https://doi.org/10.1080/19491034.2021.1889858>



© 2021 The Author(s). Published by Informa UK Limited, trading as Taylor & Francis Group.



[View supplementary material](#)



Published online: 04 Mar 2021.



[Submit your article to this journal](#)



Article views: 1333



[View related articles](#)





[View Crossmark data](#)





Citing articles: 2 [View citing articles](#)

RESEARCH PAPER

 OPEN ACCESS 

## HP1 $\beta$ carries an acidic linker domain and requires H3K9me3 for phase separation

Weihua Qin<sup>a</sup>, Andreas Stengl<sup>a</sup>, Enes Ugur<sup>a,b</sup>, Susanne Leidescher<sup>a</sup>, Joel Ryan<sup>a</sup>, M. Cristina Cardoso <sup>c</sup>, and Heinrich Leonhardt <sup>a</sup>

<sup>a</sup>Center for Molecular Biosystems (BioSysM), Faculty of Biology, Ludwig-Maximilians-Universität München, Munich, Germany; <sup>b</sup>Department of Proteomics and Signal Transduction, Max Planck Institute for Biochemistry, Martinsried, Germany; <sup>c</sup>Cell Biology and Epigenetics, Department of Biology, Technical University of Darmstadt, Darmstadt, Germany

### ABSTRACT

Liquid-liquid phase separation (LLPS) mediated formation of membraneless organelles has been proposed to coordinate biological processes in space and time. Previously, the formation of phase-separated droplets was described as a unique property of HP1 $\alpha$ . Here, we demonstrate that the positive net charge of the intrinsically disordered hinge region (IDR-H) of HP1 proteins is critical for phase separation and that the exchange of four acidic amino acids is sufficient to confer LLPS properties to HP1 $\beta$ . Surprisingly, the addition of mono-nucleosomes promoted H3K9me3-dependent LLPS of HP1 $\beta$  which could be specifically disrupted with methylated but not acetylated H3K9 peptides. HP1 $\beta$  mutants defective in H3K9me3 binding were less efficient in phase separation *in vitro* and failed to accumulate at heterochromatin *in vivo*. We propose that multivalent interactions of HP1 $\beta$  with H3K9me3-modified nucleosomes via its chromodomain and dimerization via its chromoshadow domain enable phase separation and contribute to the formation of heterochromatin compartments *in vivo*.

### ARTICLE HISTORY

Received 10 October 2020  
Revised 6 February 2021  
Accepted 8 February 2021

### KEYWORDS





Phase separation; chromatin structure; heterochromatin; histone posttranslational modification; heterochromatin binding protein HP1

## Introduction

Liquid-liquid phase separation (LLPS) has recently emerged as a novel form of the cellular organization [1–4]. In addition to canonical membrane-bound organelles, phase separation forms membraneless organelles within cells to compartmentalize complex biological reactions in space and time. The formation of membraneless organelles is driven by intrinsically disordered proteins or disordered protein regions (IDR) [5,6]. Those proteins or protein domains are characterized by a low content of hydrophobic amino acids, biased amino acid composition, and low sequence complexity [5,7–10]. The cellular abundance of disordered proteins is tightly regulated and mutations in those proteins or changes in their cellular abundance are often associated with disease [11,12].

Heterochromatin binding protein HP1 is a non-histone chromosome binding protein and has a function in nuclear organization, chromosome segregation, telomere maintenance, DNA repair, and gene silencing [13,14]. In mammals, there

are three homologs of HP1, termed HP1 $\alpha$ , HP1 $\beta$ , and HP1 $\gamma$ , encoded by the genes *Cbx5*, *Cbx1*, and *Cbx3*, respectively. HP1 homologs have two conserved functional domains, an N-terminal chromodomain (CD) and a C-terminal chromoshadow domain (CSD), linked by a hinge region. The CD domain mediates recognition of di- and trimethylated K9 of histone H3 (H3K9me2 and H3K9me3) [15–17], while the CSD domain is responsible for interaction with other proteins and also mediates homo- and hetero-dimerization [18,19]. The intrinsically disordered regions and posttranslational modifications are likely responsible for the unique functions of HP1 homologs. Recent studies testing the capacity of HP1 to induce phase separation revealed that only HP1 $\alpha$  formed phase-separated droplets [20–22]. This phase separation is initiated through intermolecular interaction of the phosphorylated N-terminus with the hinge region and correlates with the formation of heterochromatin and chromocenters in the nucleus.

**CONTACT** Weihua Qin  [weihua@zi.biologie.uni-muenchen.de](mailto:weihua@zi.biologie.uni-muenchen.de); Heinrich Leonhardt  [h.leonhardt@lmu.de](mailto:h.leonhardt@lmu.de)  Center for Molecular Biosystems (BioSysM), Faculty of Biology, Ludwig-Maximilians-Universität München, Butenandtstraße 1, Munich D-81377, Germany  
 Supplemental data for this article can be accessed [here](#).

© 2021 The Author(s). Published by Informa UK Limited, trading as Taylor & Francis Group.  
This is an Open Access article distributed under the terms of the Creative Commons Attribution License (<http://creativecommons.org/licenses/by/4.0/>), which permits unrestricted use, distribution, and reproduction in any medium, provided the original work is properly cited.

Although HP1 $\beta$  also predominantly accumulates at pericentromeric heterochromatin (chromocenters), it does not form phase-separated droplets under the conditions described for HP1 $\alpha$ . It is though not clear how much LLPS mechanisms contribute to heterochromatin formation and clustering and, indeed, a model polymer-polymer/liquid-phase separation (PPPS or PLPS) has been recently proposed [23,24].

Chromatin organization undergoes dramatic changes during mammalian cell differentiation and proliferation. In proliferating cells, heterochromatin clusters (chromocenters) are disrupted during mitosis as they contain clustered centromeric and pericentromeric DNA from several chromosomes and then fuse again throughout interphase reaching the highest clustering in G2 and in terminally differentiated post-mitotic cells [25]. This fusion of chromocenters *in vivo* resembles the formation of phase-separated droplets *in vitro* and depends on the presence and concentration of heterochromatin proteins like HP1 $\alpha$  and MeCP2 [20,22,25]. At the transition from pluripotent to differentiated stages, heterochromatin foci become more clustered and spherical [25,26], which correlates with lower exchange rates of chromatin proteins. HP1 proteins form homo- or hetero-dimers and have often been considered to play a rather equivalent role in heterochromatin organization. However, several lines of evidence suggest that the different HP1 proteins have specific functions in heterochromatin organization. For example, it has been shown that HP1 $\alpha$  plays an important role in heterochromatin organization, while HP1 $\beta$  functionally associates with H4K20me3 [27,28]. HP1 $\beta$  has been suggested to act as a bridge linking H3K9me3 enriched condensed chromatin [29]. In addition, HP1 $\alpha$  and HP1 $\beta$  likely play distinct roles during early embryo development, as they show different expression patterns [30].

To dissect functional differences of HP1 homologs in phase separation and chromatin organization, we compared the amino acid composition of HP1 proteins at disordered regions. We found that the charge of the IDR-H is a distinctive feature of HP1 homologs and plays a decisive role in LLPS and that HP1 $\beta$  undergoes phase separation in a histone

H3K9me3 dependent manner. Hence, an HP1 $\beta$  mutant defective in H3K9me3 binding was deficient in phase separation and showed faster binding kinetics *in vivo*.

## Materials and methods

### Cell culture and transfection

Mouse E14 ESCs, cells were cultured in gelatinized flasks in DMEM supplemented with 16% fetal calf serum, 0.1 mM  $\beta$ -mercaptoethanol (ThermoFisher Scientific, Invitrogen), 2 mM L-glutamine, 1 $\times$  MEM non-essential amino acids, 100 U/ml penicillin, 100  $\mu$ g/ml streptomycin (Sigma-Aldrich, Germany), 2i (1  $\mu$ M PD032591 and 3  $\mu$ M CHIR99021 (Axon Medchem, Netherlands) and 1000 U/ml recombinant leukemia inhibitory factor LIF (Millipore). Human embryonic kidney (HEK) 293 T cells were cultured in DMEM supplemented with 10% fetal calf serum and 50  $\mu$ g/ml gentamycin (PAA).

Mouse ESCs were transfected with Lipofectamine 3000 Reagent (ThermoFisher Scientific, Invitrogen) according to the manufacturer's instructions.

### CRISPR/Cas-mediated gene editing and generation of stable cell lines

For the generation of GFP-HP1 $\beta$  WT and KW cell lines, the MINtag strategy was used as described previously [31]. In brief, HP1 $\beta$  specific gRNA was cloned into a vector expressing GFP and SpCas9 (px458: F. Zhang Lab). Mouse ESCs were transfected with the Cas9-gRNA vector and a 200 nt donor oligo coding for the MINtag. Two days after transfection, GFP positive cells were separated using FACS (Becton Dickinson, Germany) and plated at clonal density (2000 cells per p100 plate). After one-week, single clones were picked manually and transferred into two 96-well plates. Cell lysis in 96-well plates, PCR on lysates, and restriction digest were performed. To generate WT and KW GFP-HP1 $\beta$  cell lines, we used our MIN-tagged HP1 $\beta$  mESCs and inserted the WT or the KW GFP-HP1 $\beta$  coding sequence into the N-terminus of the endogenous *HP1 $\beta$ <sup>attP/attP</sup>* locus by Bxb1

mediated recombination (Figure 5d). PCR primers for screening are as follows:

HP1 $\beta$ -ext F: 5'-GATTTCCCTGGGCTCCTC  
AC-3'

HP1 $\beta$ -ext R: 5'-ATGCCCATCACAGAAGCTG  
CT-3'

AttL-F: 5'- CCGGCTTGTCGACGACG-3'.

### **Protein purification, histone, and mononucleosome isolation**

HP1 cDNA was cloned into a pET28a (+) expression vector (Merck KGaA, Novagen), mutants were made using overlap extension PCR, and proteins were subsequently expressed in *E. coli*. For protein purification, BL21 cells were grown to OD 0.6–0.8 at 37°C, then IPTG was added to a final concentration of 0.5 mM and cultures were incubated at 18°C overnight. Harvested cells were resuspended in lysis buffer (20 mM Tris-HCl pH 8.2, 250 mM NaCl, 20 mM Imidazole, 3 mM  $\beta$ -Mercaptoethanol, 1 mM PMSF, 25  $\mu$ g/ml DNase I and 100  $\mu$ g/ml Lysozyme) and incubated at 4°C under constant rotation for 1–2 h. Following sonication, cell debris was removed by centrifugation at 20,000 x g for 30 min at 4°C. Clarified lysate was injected into an ÄKTA Purifier system (GE Life Sciences, Germany) equipped with a Ni-NTA column and His-tagged proteins were finally eluted in elution buffer (20 mM Tris/HCl pH 8.2, 250 mM NaCl, 500 mM Imidazole, and 3 mM  $\beta$ -Mercaptoethanol). The fractions with the highest purity were mixed and concentrated to about 1  $\mu$ g/ $\mu$ l using Amicon® Ultra 4 mL centrifugal filter (Merck, Germany) in the buffer (20 mM HEPES pH 7.2, 200 mM KCl, 1 mM DTT, 10% glycerol) before flash freezing in liquid nitrogen. Protein concentrations were measured with the Pierce™ 660 nm protein assay kit (ThermoFisher Scientific) according to the manual.

Histone isolation was conducted as previously described with minor changes of the protocol [33]. In brief, 15 p100 plates of HEK293T cells were harvested and cell pellets were resuspended in a hypotonic buffer (10 mM Tris-HCl pH 8, 10 mM KCl, 1.5 mM MgCl<sub>2</sub>, 1 mM DTT, and 1x Protease Inhibitor, 2 mM PMSF). To obtain pure nuclei, cells were disrupted using a homogenizer and nuclei were subsequently incubated in a chromatin dissociation buffer (10 Tris-HCl pH

8.0, 20 mM EDTA, and 400 mM NaCl) for 30 min on ice. This chromatin dissociation step was repeated 4x. Afterward, nuclei were resuspended in 0.4 N H<sub>2</sub>SO<sub>4</sub> and incubated on a rotator at 4°C overnight. After centrifugation, histones in the supernatant were transferred into a fresh reaction tube and precipitated using 33% trichloroacetic acid (TCA). After washing 3x with cold acetone, histones were dissolved in H<sub>2</sub>O and centrifuged at 2000 rpm for 5 min to remove precipitates. Histone concentrations were measured using the Pierce™ 660 nm protein assay kit.

For isolation of mononucleosomes,  $3 \times 10^7$  HEK293T cells were resuspended in 1 ml of hypotonic buffer containing 0.1% Triton-X 100, homogenized with 20 strokes in a Glass Teflon homogenizer and centrifuged at 1000 x g at 4°C to obtain intact nuclei. Nuclei were then resuspended in 800  $\mu$ l of MNase digestion buffer (10 mM Tris-HCl, pH 7.4, 10 mM NaCl, 3 mM CaCl<sub>2</sub>, 0.1% NP-40, and protease inhibitors) supplemented with 40 U/ml MNase and incubated at 37°C for 5 min. The digestion was inactivated by a 5x stop buffer containing 10 mM Tris-HCl, pH7.4, 710 mM NaCl, and 7.5 mM EDTA. Mononucleosome extracts were cleared by centrifugation at 2 000 x g for 15 min at 4°C and the quality of the preparation was determined on an agarose gel after isolating DNA from the mononucleosome extracts.

### **In vitro droplet assays**

For the droplet assay, proteins were concentrated to ~10  $\mu$ g/ $\mu$ l using Amicon® Ultra 4 mL centrifugal filter (Merck, Germany). After the concentration step, the buffer was exchanged to 20 mM HEPES pH 7.2, 75 mM KCl, 1 mM DTT with Zeba™ Spin Desalting Columns, and 1.4 nmol of HP1 $\beta$  were mixed with 1.4 nmol of histones in a total of 30  $\mu$ l buffer at 4°C. 20  $\mu$ l of the turbid solution was imaged in a 15  $\mu$ -Slide 18 Well ibidi chamber. Differential interference contrast (DIC) images were acquired on a DeltaVision Personal widefield microscope (GE Life Sciences) equipped with a 60  $\times$  1.42 NA objective (Olympus), LED epi-illumination, and a CoolSnap ES2 camera (Photometrics).

For the spin-down assay, 30  $\mu$ l of the turbid solution was spun down at 2000 rpm for 5 min

and 29  $\mu\text{l}$  of supernatant was transferred into a Protein LoBind Tube (Eppendorf). The supernatant and droplets were boiled in 250  $\mu\text{l}$  Laemmli loading buffer at 95°C for 10 min. 5  $\mu\text{l}$  of supernatant and droplets were loaded into an SDS-PAGE gel followed by either detection using coomassie staining or western blot analysis.

For HP1 $\beta$  phase separation with mononucleosome extracts, 28  $\mu\text{l}$  of extract were incubated with 30  $\mu\text{g}$  of HP1 $\beta$  in 30  $\mu\text{l}$  solution for 5 min and spun down at 12,000 rpm for 5 min. 29  $\mu\text{l}$  of supernatant was transferred into a Protein LoBind Tube and both supernatant and droplets were boiled in 40  $\mu\text{l}$  Laemmli loading buffers at 95°C for 10 min. 20  $\mu\text{l}$  of supernatant and droplets were again loaded into an SDS-PAGE gel followed by either detection using Coomassie staining or western blot analysis.

For comparison of histones and H3 peptides in HP1 $\beta$  phase separation, H3 peptides (aa 1–20) carrying H3K9me3 and biotinylated at the C-terminus were purchased from PSL GmbH, Heidelberg.

For the peptide competition assay, 25  $\mu\text{M}$  of HP1 $\beta$  was incubated for 1 h with C-terminal TAMRA labeled histone H3 peptides (aa 1–20), containing H3K9me3, H3K9me1 or H3K9ac (PSL GmbH, Heidelberg) in a ratio of 1:5 or 1:50 in 30  $\mu\text{l}$  buffers in Protein LoBind Tubes at 4°C. Then, 25  $\mu\text{M}$  of histones were added to the solution and incubated at 4°C for 3 min. Droplets were separated by centrifugation at 2000 rpm for 5 min and 29  $\mu\text{l}$  of supernatant were transferred into a new microfuge tube. Supernatant and droplets were boiled in 200  $\mu\text{l}$  Laemmli loading buffers at 95°C for 10 min and 6  $\mu\text{l}$  of each sample was loaded into an SDS-PAGE gel for detection by coomassie staining and TAMRA fluorescence.

### **Analytic ion-exchange chromatography (IEX) and size-exclusion chromatography (SEC)**

The surface charge of HP1 variants was analyzed by anion exchange chromatography. 50  $\mu\text{g}$  HP1 $\alpha$ , HP1 $\beta$ , or HP1 $\gamma$  were diluted in 500  $\mu\text{l}$  buffer A (20 mM Tris-HCl, pH 8.0) and loaded on a 1 mL Resource Q column at room temperature and 4 ml/min flow rate using a Äkta Pure FPLC system. Samples were eluted with a linear gradient over 20 column volumes (CV) to 50% buffer B (20 mM Tris-HCl, 1 M NaCl, pH 8.0) followed

by 10 CV 100% buffer B. Absorption at 280 nm was recorded.

250  $\mu\text{g}$  of extracted histones were diluted in 50  $\mu\text{l}$  SEC running buffers (20 mM Tris-HCl, 300 mM NaCl, pH 7.4). The sample was separated on an equilibrated Superdex 200 Increase 10/300 GL column at room temperature and 0.75 ml/min flow rate using a Äkta Pure FPLC system. Absorption at 280 nm was recorded. For size comparison, a protein gel filtration marker mix (Sigma-Aldrich) including carbonic anhydrase (29 kDa), bovine serum albumin (66 kDa), alcohol dehydrogenase (150 kDa), beta-amylase (200 kDa), apoferritin (443 kDa), thyroglobulin (669 kDa) was analyzed under identical conditions.

### **Antibodies for western blot analysis**

Primary antibodies used for western blot, including the polyclonal rabbit anti-H3 (Cat # ab1791), anti-H3K9me3 (Cat # ab8898), and anti-HP1 $\beta$  (Cat #10478) antibodies, were purchased from Abcam and the secondary antibody, anti-rabbit-IgG AF647 (Cat # A32733), from Invitrogen. The primary mouse monoclonal anti-H1 antibody (H-2) was purchased from Santa Cruz Biotechnology (Cat # sc-393358) and the secondary antibodies, anti-mouse IgG-HRP (Cat # A9044), and anti-rabbit IgG-HRP (Cat # A6154) were purchased from Sigma-Aldrich.

### **Immunofluorescence staining**

mESCs were washed with phosphate-buffered saline (PBS) and fixed with 3.7% formaldehyde in PBS, permeabilized with 0.5% Triton X-100 in PBS, and then blocked with 3% BSA. Cells were then incubated with a rabbit polyclonal anti-H3K9me3 antibody (Abcam, Cat # ab8898) or a rabbit polyclonal anti-HP1 $\beta$  antibody (Abcam, Cat #10478) for 1 hour at RT. After washing, cells were incubated with Alexa594-conjugated donkey anti-rabbit IgG secondary antibody (Invitrogen, Cat # A21207) for H3K9me3 and Alexa488-conjugated goat anti-rabbit IgG (Invitrogen, Cat # A11034) for HP1 $\beta$  1 hour at RT. Nuclei were stained with 4',6-diamidino-2-phenylindole (DAPI) and mounted on coverslips with Vectashield (Vector Laboratories). Images were taken using an SP5 Leica confocal microscope equipped with Plan Apo 63x/1.4 NA oil immersion objective and lasers with excitation



lines: 405 nm for DAPI, 488 nm for HP1 $\beta$  and GFP-HP1 $\beta$ , and 594 nm for H3K9me3.

### FRAP analysis

FRAP experiments were performed on an UltraVIEW VoX spinning disc microscope with an integrated FRAP PhotoKinesis accessory (PerkinElmer) assembled onto an Axio Observer D1 inverted stand (Zeiss) and using a 100 $\times$ /1.4 NA Plan-Apochromat oil immersion objective. The microscope was equipped with a heated environmental chamber set to 37 $^{\circ}$ C. Fluorophores were excited with a 488 nm solid-state diode laser line. Confocal image series were typically recorded with 16-bit image depth, a frame size of 512  $\times$  512 or 256  $\times$  256 pixels, and a pixel size of 69 nm. The bleach regions, typically with a diameter of 2  $\mu$ m, were manually chosen to cover chromocenters. Photobleaching was performed using one iteration with the acousto-optical tunable filter (AOTF) of the 488 nm

laser line set to 100% transmission. Twenty prebleach images were acquired at maximum speed, then 60 post-bleach frames were recorded at maximum speed followed by 30 frames at a rate of 3 s per frame. Data correction, normalization, and quantitative evaluations were performed by processing with ImageJ (<http://rsb.info.nih.gov/ij/>) followed by calculations in Excel. For normalization, the average intensity of five prebleach images was used.

## Results

### HP1 $\beta$ differs from HP1 $\alpha$ and HP1 $\gamma$ in that it contains an acidic linker domain

Although the three HP1 homologs are very similar in their overall structure, only HP1 $\alpha$  was reported to undergo LLPS [20]. As LLPS involves intrinsically disordered regions (IDRs) of proteins, we scrutinized and compared the disordered regions of HP1 proteins (Figure 1a). The

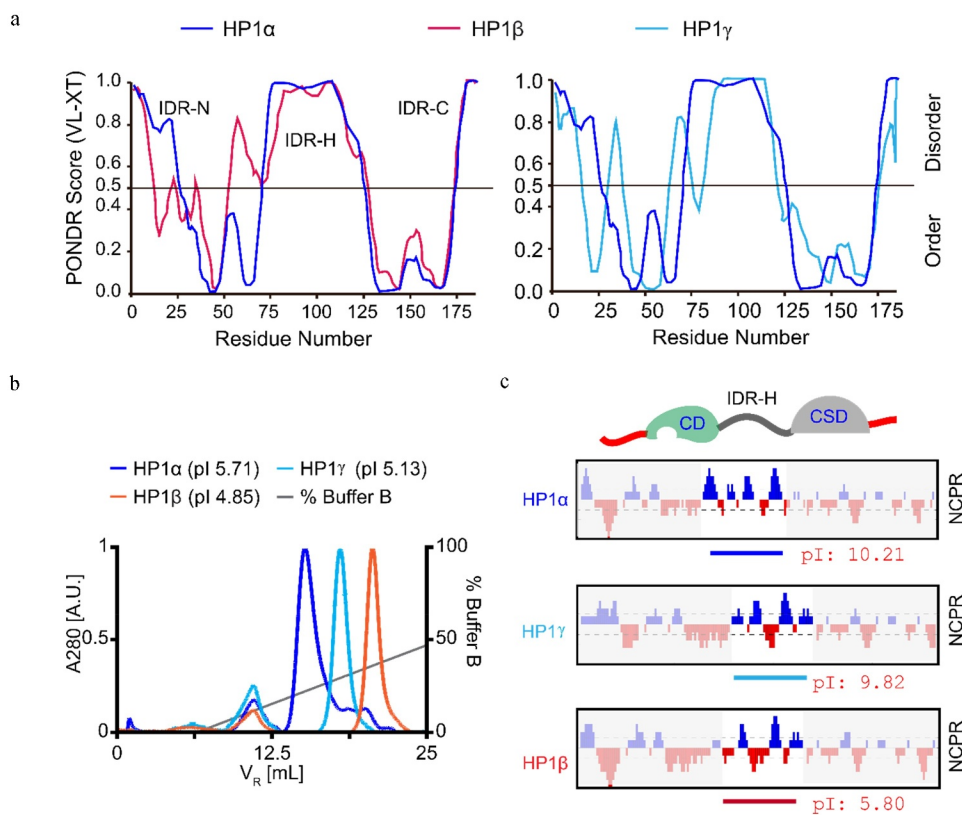


**Figure 1.** HP1 $\beta$  differs from HP1 $\alpha$  and HP1 $\gamma$  in that it contains an acidic linker domain. (a) Comparison of order/disorder prediction of HP1 homologs by the PONDR algorithm, a website tool (<http://www.pondr.com/>). VLXT scores are shown on the y-axis, amino acid positions are shown on the x-axis. (b) Ion exchange chromatography analysis of HP1 proteins. 50  $\mu$ g of HP1 proteins were diluted in 500  $\mu$ L buffer B (20 mM Tris-HCl, pH 8.0) and loaded on a 1 mL Resource Q column and analyzed by using a Äkta Pure FPLC system. (c) Net charge distribution per residue (NCPR) of HP1 proteins (CIDER, pappulab.wustl.edu). Negatively charged amino acids are marked in red, positively charged amino acids in blue. The pI of IDR-H in HP1 proteins is indicated.

C-terminal disordered region (IDR-C) was relatively conserved and only minor differences were observed at the N-terminus (IDR-N) and hinge region (IDR-H) (Figure 1a). However, HP1 homologs have different theoretical isoelectric points (pI). To investigate the HP1 proteins *in vitro*, we induced the expression of His tagged HP1s in *E. coli* and purified them using a Ni-NTA column. Purified HP1 proteins were checked by coomassie blue-stained SDS-PAGE gels (Figure S1A) and showed the expected protein sizes, HP1 $\alpha$  (24.3 kDa), HP1 $\beta$  (23.7 kDa), and HP1 $\gamma$  (23.0 kDa). Then, we performed ion-exchange chromatography analysis and confirmed the expected pI of HP1 proteins (Figure 1b). Among the three homologs, HP1 $\beta$  is the most acidic protein (pI 4.85), followed by HP1 $\gamma$  (pI 5.13) and HP1 $\alpha$  (pI 5.71) (Figure 1b). Further analysis revealed that this difference between HP1 homologs was most pronounced in the IDR-H. Whereas HP1 $\alpha$  and HP1 $\gamma$  contain more positively than negatively charged residues in their IDR-H (15/6 and 13/8, respectively), HP1 $\beta$  has relatively equal numbers of positively and negatively charged residues (11/12) in the IDR-H resulting in a much lower local pI of 5.80 (Figure 1c).

### HP1 $\beta$ cannot self-phase separate because of its acidic linker domain

We next systematically compared the property of HP1 homologs in phase separation. In the absence of IDR-N phosphorylation and DNA, we observed LLPS with HP1 $\alpha$  at 200  $\mu$ M and to a lesser extent at 50  $\mu$ M, both at 4°C (Figure 2a). While HP1 $\gamma$  underwent LLPS at a higher concentration (900  $\mu$ M at 4°C); HP1 $\beta$  did not at any of these conditions (Figure 2a). As the most distinguishing feature of HP1 $\beta$  is the acidic rather than basic IDR-H, we next replaced four acidic amino acids in IDR-H, including aspartic acid (D) 88, D90, glutamic acid (E) 92, and D93, with lysine (K) or arginine (R) (HP1 $\beta$  RKRK). Indeed, this engineered HP1 $\beta$  RKRK could form phase-separated droplets at concentrations as low as 170  $\mu$ M at 4°C (Figures 2b and S1B) underscoring the decisive role of the basic IDR-H in LLPS. The size of the HP1 $\beta$  RKRK droplets was comparable with the HP1 $\alpha$  droplets at the concentration of 200  $\mu$ M (Figure 2a). As the self-phase separation of HP1 proteins is mediated by the interaction of IDR-N and IDR-H [20,22], we analyzed the correlation between the charge ratio of IDRs and HP1 protein concentration at which phase separation was observed. With a linear function fitting, we

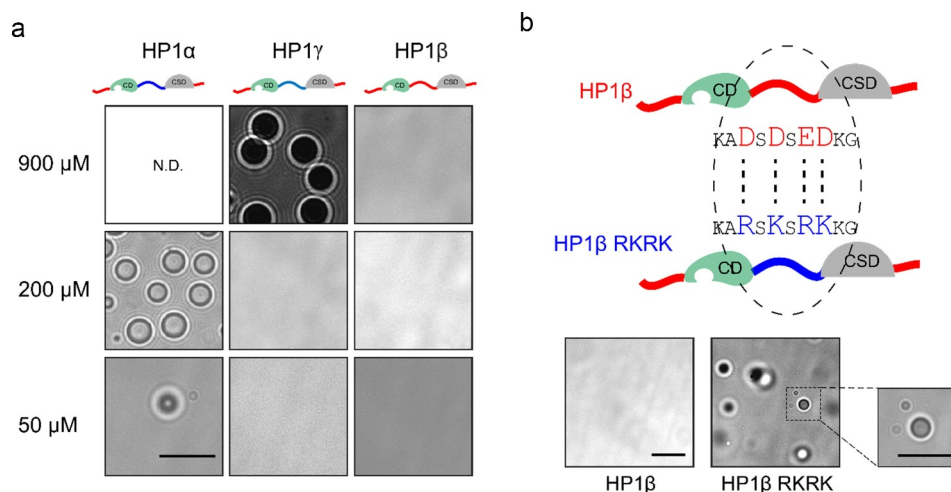


**Figure 2.** HP1 $\beta$  cannot self-phase separate because of its acidic linker domain. (a) DIC images of HP1 droplets at 4°C in a buffer containing 20 mM HEPES pH 7.2, 75 mM KCl and 1 mM DTT using the 63x objective of a DeltaVision Personal Microscope (scale bar: 10  $\mu$ m). Protein concentrations are as indicated. N.D.: not done. (b) Phase separation of engineered HP1 $\beta$  at 170  $\mu$ M and 4°C with four amino acid substitutions in the IDR-H changing it from acidic to basic (HP1 $\beta$  RKRK). A zoomed-in image is shown with the same magnification as in (a). Scale bar: 10  $\mu$ m.

obtained an estimated concentration of HP1 $\beta$  self-phase separation of  $\sim 1.736$  mM (Figure S2).

### **HP1 $\beta$ can form phase-separated droplets in the presence of histones**

These results show that HP1 $\beta$  by itself hardly undergoes LLPS *in vitro*, but then again it interacts with numerous cellular proteins, which will likely affect and modulate its properties. As the most prominent known interactors are histone tails, we isolated mononucleosomes from HEK293T cells by MNase digestion (Figures 3a and S3). To isolate pure mononucleosomes, we first titrated the MNase concentration from 1.25 to 160 U/ml and used 40 U/ml for the preparation of mononucleosomes (Figure S3A and S3B). We incubated HP1 $\beta$  with isolated mononucleosomes, collected phase-separated droplets by centrifugation, and analyzed the precipitates by coomassie stained SDS-PAGE gel and western blot (Figures 3b and S4A). These results suggest that mononucleosomes promote HP1 $\beta$  phase separation as evidenced by an enrichment together with core histones in the pellet fraction.

To further examine the histone mediated phase separation, we prepared histones from human HEK293T cells by following an acid-extraction protocol [32]. We directly compared the three HP1 homologs and found that at low concentrations (50  $\mu$ M) HP1 $\alpha$  and HP1 $\gamma$  did not form phase-separated droplets with histones (Figure 3c). However, HP1 $\beta$  mixed with histones yielded an opalescent solution containing spherical droplets (Figure 3c) that fused over time, which is a central criterion for LLPS (Video S1).

Toward a mechanistic understanding of HP1 $\beta$  phase separation, we investigated the influence of protein and salt concentration on droplet formation in the presence of histones. To do so, we incubated different concentrations of HP1 $\beta$  protein (3 to 100  $\mu$ M) with 100  $\mu$ M of histones at 4°C in a buffer containing 20 mM HEPES pH 7.2, 75 mM KCl and 1 mM DTT. HP1 $\beta$  phase-separated droplets were then separated by centrifugation for visualization by coomassie stained SDS-PAGE gels (Figures 3d, S4B and S4C). As a control, we incubated BSA with histones at the same conditions and did not observe phase-separated droplets at any of the conditions (Figure S4D and S4E). However, in the presence

of histones, HP1 $\beta$  solutions became turbid starting at concentrations as low as 25  $\mu$ M, showing characteristic phase-separated droplets (Figures 3d, S4B and S4C). Droplets with 50  $\mu$ M HP1 $\beta$  and stoichiometric amounts of histones formed up to 400 mM NaCl became smaller with increasing salt concentrations and disappeared at 600 mM NaCl (Figures 3e, S5A, S5B and summarized in Figure 3f). These results indicate that HP1 $\beta$  undergoes LLPS under physiological salt and protein concentrations.

### **Trimethylation of K9 of histone H3 and histone dimerization are required for HP1 $\beta$ phase separation**

Previously it was reported that linker histone H1 forms LLPS with DNA and nucleosomes [33–35]. To investigate the contribution of histone H1 to HP1 $\beta$  phase separation, we analyzed phase-separated droplets by western blot. We clearly detected histone H1 in the supernatants, but not in pellets of HP1 $\beta$  phase-separated droplets (Figure S6). This result suggests that histone H1 is not required for HP1 $\beta$  phase separation.

When incubating increasing concentrations of HP1 $\beta$  with purified core histones, we found first histone H3 (in particular the trimethylated K9 form, H3K9me3) in droplets starting at 25  $\mu$ M with a corresponding depletion from the supernatants (Figures 3d, Figures 4a and S7A), while at higher concentrations also the other core histones (H2A, H2B, and H4) were present (Figure 3d). While core histones were sufficient for HP1 $\beta$  LLPS, we found that H3K9me3 peptides encompassing amino acids 1–20 (aa 1–20), the binding substrate of the HP1 $\beta$  CSD, did not cause turbidity and droplet formation (Figure 4b). The fact that H3K9me3 histone tails were not sufficient for HP1 $\beta$  LLPS suggests that the remainder of the H3 histone, in particular the histone fold domains, and their ability to dimerize are required for LLPS. Indeed, size-exclusion chromatography (SEC) of histone preparations showed a major peak between 29 and 66 kDa, likely corresponding to a histone dimer (Figure 4c). We, next, performed a competition assay using H3 peptides containing either K9me3, or K9me1, or K9ac modifications added to the HP1 $\beta$  and histones (Figure 4d and



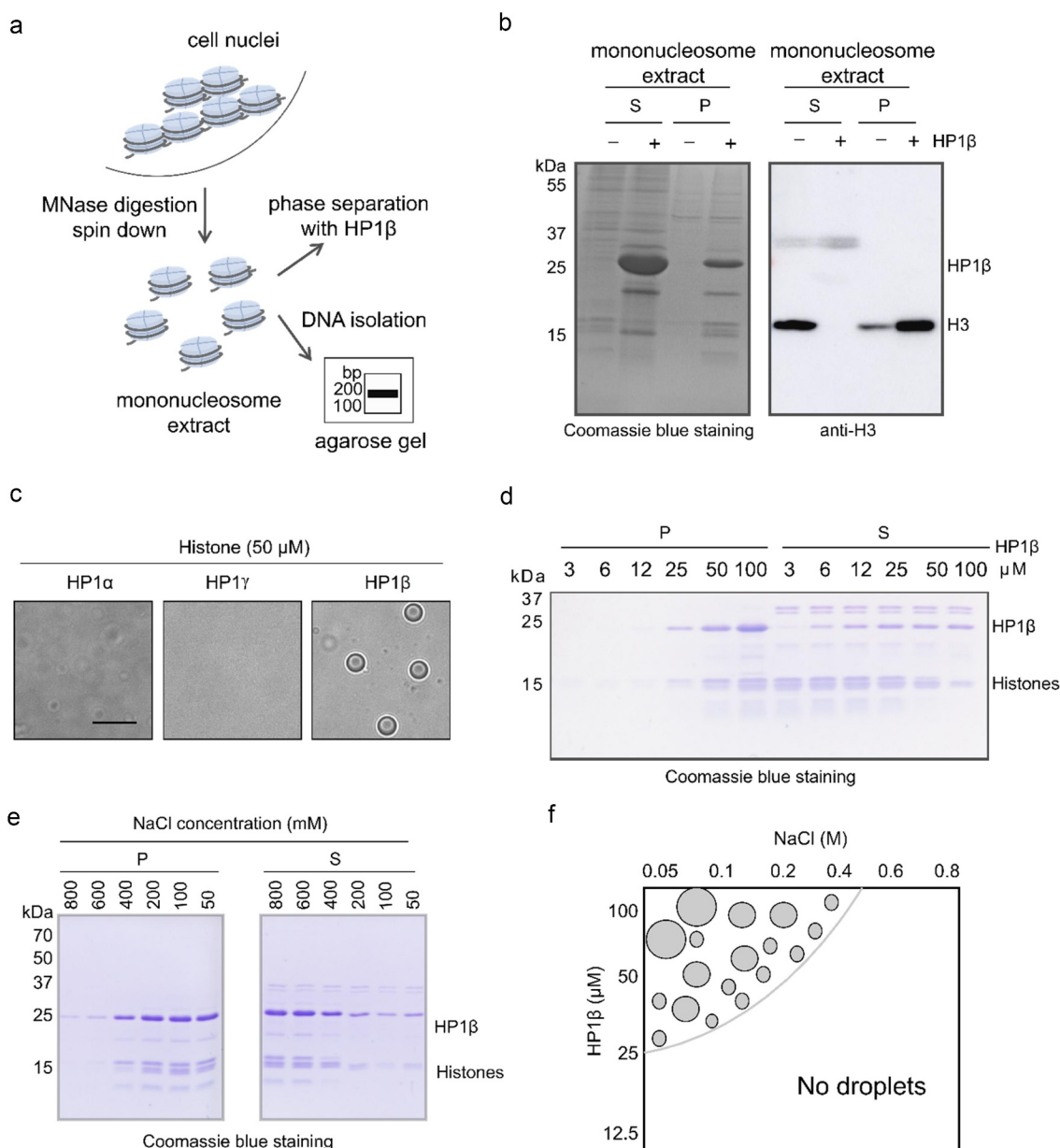


**Figure 3.** HP1β can form phase-separated droplets in the presence of histones. (a) Illustration of isolating mononucleosomes by MNase treatment (left). (b) Mononucleosome solution was incubated with or without 30 μg of HP1β at 4°C in a buffer containing 20 mM Tris-HCl pH 7.5, 150 mM NaCl, 3 mM CaCl<sub>2</sub>, 0.1% NP-40 and 1.5 mM EDTA. Phase-separated droplets were pelleted by centrifugation. Proteins in the supernatant (S) and phase-separated droplets (P) were separated and visualized by coomassie blue SDS-PAGE gels and western blotting with an anti-H3 antibody. (c-e) HP1 phase separation in the presence of histones isolated by acid-extraction from HEK293T cells in a buffer of 20 mM HEPES pH 7.2, 75 mM KCl and 1 mM DTT. 50 μM of HP1 homologs were incubated with 50 μM of histones (scale bar: 10 μm) (c). 3 to 100 μM of HP1β was incubated with 100 μM of histones. HP1β phase-separated droplets were separated and visualized as above (d). 50 μM of HP1β was incubated with 50 μM of histones in a buffer with NaCl concentrations ranging from 50 to 800 mM. Proteins in the P and S fractions were analyzed as above (e). (f) Phase diagram of HP1β with protein and salt concentration as order parameters. Phase separation was scored by the presence or absence of droplets in the sample.

S7B). Notably, only H3K9me3 peptides, but not H3K9me1 and H3K9ac peptides, efficiently disrupted HP1β-histone dependent LLPS.

The amino acids in the CD domain, including tyrosine (Y) 21, tryptophan (W) 42, and phenylalanine (F) 45, form an aromatic cage for H3K9me3

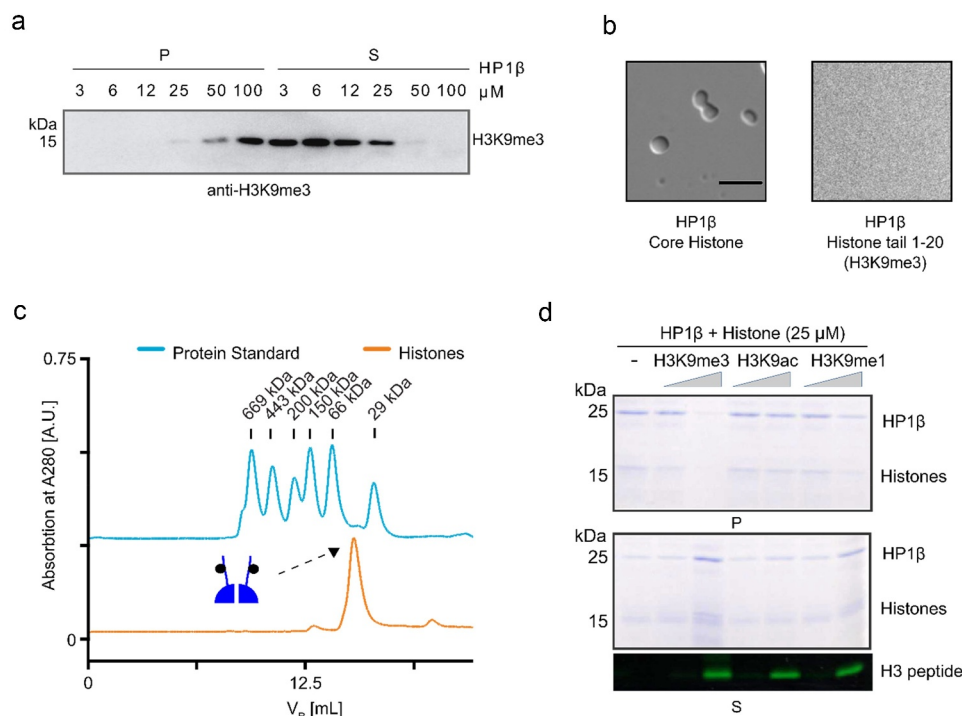


**Figure 4.** Trimethylation of K9 of histone H3 (H3K9me3) and histone dimerization are required for HP1 $\beta$  phase separation. (a) HP1 $\beta$  protein from 3 to 100  $\mu$ M was incubated with 100  $\mu$ M of histones at 4 $^{\circ}$ C in a buffer containing 20 mM HEPES pH 7.2, 75 mM KCl and 1 mM DTT. HP1 $\beta$  phase-separated droplets were separated by spin down. Proteins in P and S fractions were analyzed by SDS-PAGE gels and visualized western blot with anti-H3K9me3 antibody. (b) Representative DIC images show HP1 $\beta$  phase separation assay outcome in the presence of histones or histone H3 peptide (aa 1–20) carrying H3K9me3. 25  $\mu$ M of HP1 $\beta$  was incubated with either 25  $\mu$ M core histones or H3K9me3 peptide (aa 1–20). (c) Analysis of histones by size exclusion chromatography (SEC). 250  $\mu$ g of histones were diluted in a buffer of 20 mM Tris-HCl, 300 mM NaCl, pH 7.4 and separated on an equilibrated Superdex 200 Increase 10/300 GL column. For size comparison a protein marker mix including carbonic anhydrase (29 kDa), bovine serum albumin (66 kDa), alcohol dehydrogenase (150 kDa), beta-amylase (200 kDa), apoferritin (443 kDa), and thyroglobulin (669 kDa) was analyzed under identical conditions. (d) Histone H3 peptide (aa 1–20) carrying H3K9me3, or H3K9me1 or H3K9ac was incubated with 25  $\mu$ M of HP1 $\beta$  and histones. Proteins in S and P fractions were analyzed and visualized by coomassie stained SDS-PAGE gels and H3 peptides by fluorescent imaging.

binding (Figure 5a). The replacement of K41 and W42 with alanine (HP1 $\beta$  KW) is sufficient to abolish the H3K9me3 binding of HP1 $\beta$  [15,16]. We purified HP1 $\beta$  KW and incubated different concentrations of the mutant proteins (6 to 25  $\mu$ M) with 25  $\mu$ M histones. By analyzing coomassie stained SDS-PAGE gels, we found that almost half of histone H3 was still detected in the supernatant of phase-separated droplets of HP1 $\beta$  KW at the concentration (12  $\mu$ M), while H3 was nearly completely depleted from the supernatant into the pellet of HP1 $\beta$  WT droplets (Figure S8A and S8B). This concentration corresponds to the physiological HP1 $\beta$  concentration measured at heterochromatin [36]. At the higher concentration (25  $\mu$ M), HP1 $\beta$  KW formed phase-separated

droplets similar to HP1 $\beta$  WT, which may be due to the unspecific binding with histones (Figure S8A and S8B). These results indicate that HP1 $\beta$  KW, which is deficient in binding H3K9me3, is less efficient in forming phase-separated droplets at physiological concentrations.

To study the function of HP1 $\beta$  phase separation *in vivo*, we generated a mouse embryonic stem cell (mESC) line carrying the GFP-HP1 $\beta$  KW mutant as well as a wild type using the MIN tag genome engineering strategy, called MINtool [31]. The MINtool allows to replace the endogenous gene of interest with the mini gene products that carry mutations or tags. With this strategy, a multifunctional integrase (MIN) tag sequence was first inserted into the open reading frame of

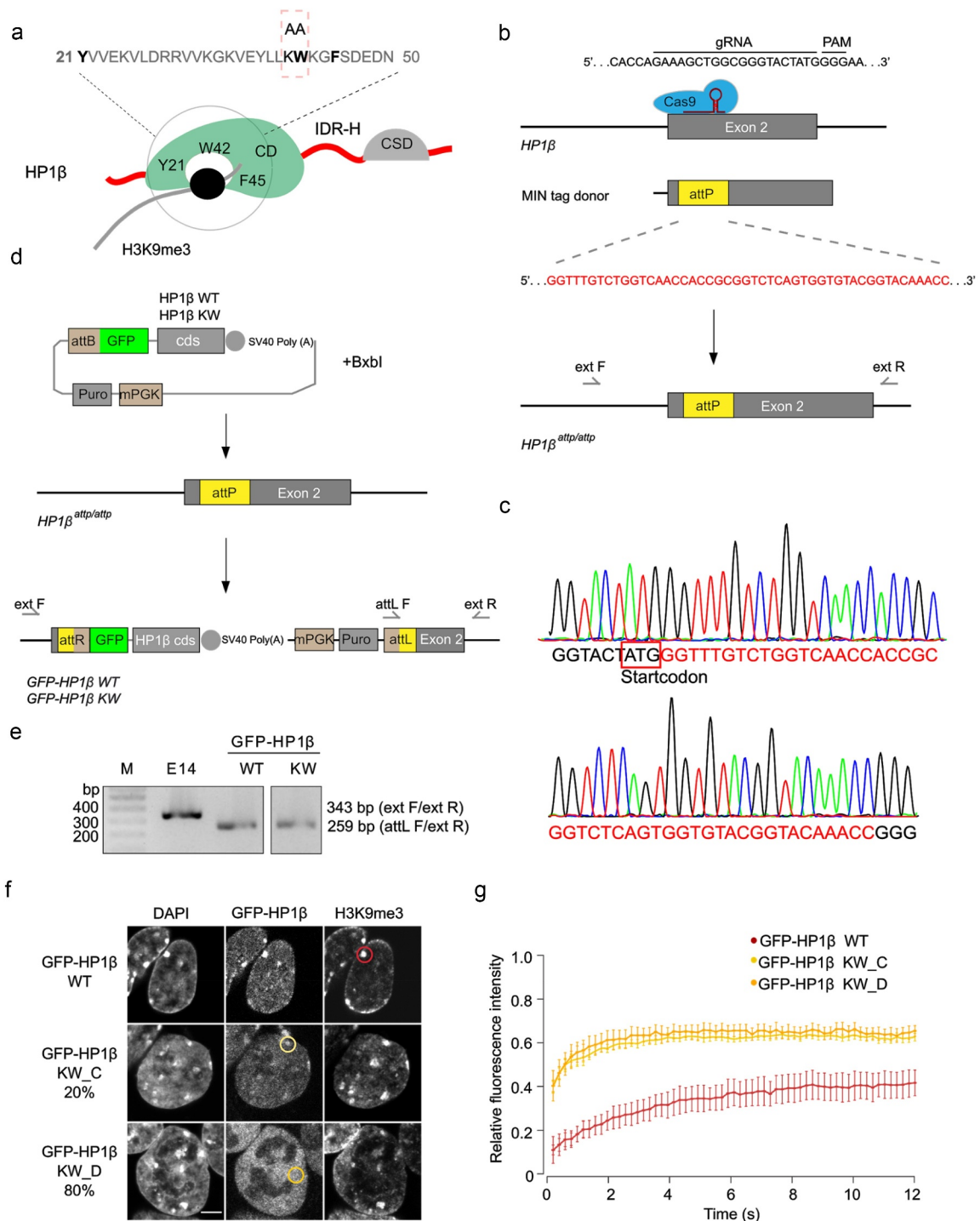


**Figure 5.** HP1β phase separation contributes to heterochromatin formation *in vivo*. (a) Illustration of the binding of H3K9me3 and the CD domain of HP1β. The amino acids, tyrosine (Y) 21, tryptophan (W) 42 and phenylalanine (F) 45, form an aromatic cage for H3K9me3 peptide that is abolished by the replacement of K41W42 with alanine (A) [15]. (b and c) Schematic representations show the CRISPR/Cas9 gene-editing strategy used to generate MIN tagged HP1β mESCs. The donor harbors the MIN tag sequence (*attP*) and homology arms to the genomic sequence 5' and 3' of the translational start site. The targeting region was amplified with primers as indicated and assessed by Sanger sequencing. (d) Schematic representation shows the strategy to generate GFP-HP1β WT and KW mESC lines with Bxb1 mediated recombination. (e) Gel electrophoresis of the multiplex PCR for validation of GFP-HP1β mESCs with primers as indicated in (d). 343 bp and 259 bp sequences were amplified from E14 and GFP-HP1β cells, respectively. (f) Representative images of GFP-HP1β WT and KW mESCs stained with an anti-H3K9me3 antibody. Scale bar: 5 μm. See overview images in Figure S10. (g) FRAP quantification of GFP-HP1β WT and GFP-HP1β KW. Curves show average GFP signal relative to the fluorescence signal prior to bleaching (WT, n = 20 and KW\_C (chromocenter), n = 6 and KW\_D (diffuse), n = 6). The areas used for FRAP are indicated by circles in (f).

HP1 $\beta$  directly downstream of the start codon by the CRISPR/Cas9 genome editing tool (Figure 5b and c). By Bxb1-mediated recombination, the coding sequences for GFP-HP1 $\beta$  WT and GFP-HP1 $\beta$  KW were subsequently integrated into the locus (Figure 5d). With specific primers, 343 bp and 259 bp sequences were amplified from the MIN tagged and GFP tagged HP1 $\beta$  cell lines, respectively (Figure 5e). We performed western blot analysis and found that the levels of GFP-HP1 $\beta$  WT and KW in the engineered cells are higher than the endogenous HP1 $\beta$  levels in WT mESCs (Figure S9). In line with previous publications, GFP-HP1 $\beta$  WT is predominantly localized at the chromocenters (Figure 5f). GFP-HP1 $\beta$  KW, on the other hand, showed a dispersed nuclear distribution (KW\_D) in 80% of the mutant cells with no accumulation at heterochromatin compartments, while it slightly accumulated at the chromocenters (KW\_C) in 20% of the cells (Figures 5f and S10). To measure the kinetics of binding in living cells, fluorescence recovery after photobleaching (FRAP) analyses were performed and evaluated. These showed a similar kinetics of recovery of GFP-HP1 $\beta$  KW\_C and KW\_D that is substantially faster than GFP-HP1 $\beta$  WT (Figure 5g).

Altogether, our results show that all three HP1 proteins can in principle form phase-separated droplets

*in vitro* but require different conditions. While LLPS of HP1 $\alpha$ /HP1 $\gamma$  mostly relies on the interaction of IDR-N and IDR-H (Figure 6), HP1 $\beta$  phase separation requires the binding of H3K9me3 nucleosomes (Figure 6). These multivalent interactions are required for the formation of oligomeric structures and phase-separated droplets *in vitro*. HP1 $\beta$  dimerization and binding of two H3K9me3 histone tails thus contribute to heterochromatin clustering *in vivo*.

## Discussion

The three HP1 homologs are considered important regulators of heterochromatin formation and spreading. HP1 $\alpha$ , but not HP1 $\beta$  and HP1 $\gamma$ , was shown to form LLPS driving heterochromatin formation [20,22], raising the question of which molecular determinants are responsible for these differences. A comparison shows that all three HP1s share a common overall structure but differ in the net charge of their IDR-H (Figure 1). We found that HP1 $\gamma$ , similar to HP1 $\alpha$ , contains a basic IDR-H and indeed forms phase-separated droplets albeit at high concentrations of about 0.9 mM, which is, however, four times higher than the 0.2 mM used for HP1 $\alpha$  and way beyond the reported physiological concentrations of about 10  $\mu$ M [36,37]. Here, we showed that HP1 $\beta$  has a slightly acidic IDR-H in contrast to the very basic one of HP1 $\alpha$  and HP1 $\gamma$ . Our further finding

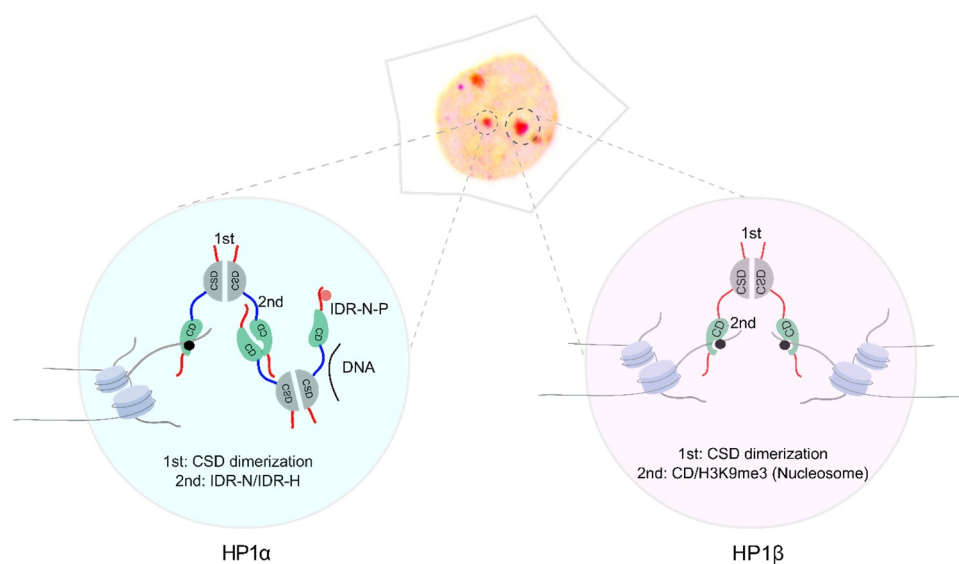


**Figure 6.** Model of HP1 $\alpha$ / $\gamma$  and HP1 $\beta$  phase separation contributing to heterochromatin formation *in vivo*. The interaction of IDR-N and IDR-H is an essential valency for HP1 $\alpha$  and HP1 $\gamma$  phase separation (left). Although HP1 $\alpha$  and HP1 $\gamma$  contain basic IDR-H, the minor difference leads to a threshold phase separation concentration higher than the physiological concentration for HP1 $\gamma$ . The negatively charged DNA and phosphorylation (P) of IDR-N can promote HP1 $\alpha$  phase separation. In contrast, HP1 $\beta$  phase separation is more complex and requires the CSD mediated dimerization and the binding of the CD domain to the H3K9me3 nucleosome (right).



that HP1 $\beta$  WT does not form phase-separated droplets, but could be engineered to do so simply by changing four acidic to basic amino acids in the IDR-H, supports the notions that HP1 $\alpha$  (and HP1 $\gamma$ ) LLPS relies on interactions between their acidic IDR-N and their basic IDR-H. Previously, it was shown that the addition of negative-charged DNA promotes the phase separation of HP1 $\alpha$  but not of HP1 $\beta$  [20,24]. Considering the difference of HP1 $\alpha$  and HP1 $\beta$  IDR-H regions, we added positive-charged histones and found that HP1 $\beta$  showed phase-separated droplets even at concentrations as low as 25  $\mu$ M. In line with our findings, it was shown that HP1 $\beta$  together with SUV39H1 forms phase-separated droplets in the presence of nuclear extracts [38]. The mode of HP1 $\beta$  LLPS differs and requires the binding of H3K9me3 nucleosomes (Figure 6). Interestingly, HP1 $\alpha$  and HP1 $\gamma$  do not phase separate under these conditions, although they have functionally similar CD domains binding H3K9me3 and a CSD for dimerization. We speculate that the interaction of their acidic IDR-N and basic IDR-H antagonizes oligomerization via histone H3K9me3 binding [39]. In any case, our study identified the net charge of the IDR-H as a critical feature controlling LLPS of HP1 *in vitro*. The observation that the simple addition of histones promotes LLPS with HP1 $\beta$  indicates that the situation *in vivo*, with its numerous direct and indirect interactions, is much more complex.

As diverse as the phase separating properties of HP1s are *in vitro*, so are their subcellular distribution and function *in vivo*. While HP1 $\gamma$  is predominantly localized in euchromatin, HP1 $\alpha$  and HP1 $\beta$  are mostly associated with heterochromatin [40]. Whereas HP1 $\alpha$  plays a central role in the formation of satellite heterochromatin, HP1 $\beta$  is involved in chromocenter formation by bridging H3K9me3 containing nucleosomes [29,41–43]. Interestingly, histone acetylation was recently described to drive LLPS and chromatin organization [33]. These results suggest that histone tail modifications in combination with specific reader proteins may encode the establishment of functionally distinct chromatin domains in the nucleus. The recent observation of HP1 independent formation of heterochromatin in cultured cell lines [24] serves as a reminder that there are several mechanisms that may cooperate or compete in the establishment of heterochromatin states

*in vivo*. Future comprehensive studies are needed to dissect their relative contributions in different cell types throughout differentiation.

## Acknowledgments

We thank Geeta Narlikar and Gary Karpen (University of California, USA) for their encouragement and comments. We thank Masahiro Muto and Haruhiko Koseki for mouse E14 WT ESCs. We thank Carina Trummer for her comments on the manuscript and Hartmann Harz for help with microscopy.



## Disclosure statement

The authors declare no competing interests.

## Funding

This work was supported by grants from the Deutsche Forschungsgemeinschaft [DFG grants SFB1064/A17 and LE 721/18-1 to H.L. and CA 198/16-1 to M.C.C.].

## ORCID

M. Cristina Cardoso  <http://orcid.org/0000-0001-8427-8859>  
Heinrich Leonhardt  <http://orcid.org/0000-0002-5086-6449>

## References

- [1] Bergeron-Sandoval LP, Safaee N, Michnick SW. Mechanisms and consequences of macromolecular phase separation. *Cell*. 2016;165:1067–1079.
- [2] Boeynaems S, Alberti S, Fawzi NL, et al. Protein phase separation: a new phase in cell biology. *Trends Cell Biol*. 2018;28:420–435.
- [3] Brangwynne CP, Eckmann CR, Courson DS, et al. Germline P granules are liquid droplets that localize by controlled dissolution/condensation. *Science*. 2009;324:1729–1732.
- [4] Hyman AA, Weber CA, Julicher F. Liquid-liquid phase separation in biology. *Annu Rev Cell Dev Biol*. 2014;30:39–58.
- [5] Kato M, Han TW, Xie S, et al. Cell-free formation of RNA granules: low complexity sequence domains form dynamic fibers within hydrogels. *Cell*. 2012;149:753–767.
- [6] Wright PE, Dyson HJ. Intrinsically disordered proteins in cellular signalling and regulation. *Nat Rev Mol Cell Biol*. 2015;16:18–29.
- [7] Alberti S, Halfmann R, King O, et al. A systematic survey identifies prions and illuminates sequence features of prionogenic proteins. *Cell*. 2009;137:146–158.
- [8] Malinowska L, Palm S, Gibson K, et al. Dictyostelium discoideum has a highly Q/N-rich proteome and shows

- an unusual resilience to protein aggregation. *Proc Natl Acad Sci U S A.* **2015**;112:E2620–2629.
- [9] Pak CW, Kosno M, Holehouse AS, et al. Sequence determinants of intracellular phase separation by complex coacervation of a disordered protein. *Mol Cell.* **2016**;63:72–85.
- [10] Wang J, Choi JM, Holehouse AS, et al. A molecular grammar governing the driving forces for phase separation of prion-like RNA binding proteins. *Cell.* **2018**;174:688–699 e616.
- [11] Aguzzi A, Altmeyer M. Phase separation: linking cellular compartmentalization to disease. *Trends Cell Biol.* **2016**;26:547–558.
- [12] Shin Y, Brangwynne CP. Liquid phase condensation in cell physiology and disease. *Science.* **2017**;357: eaaf4382.
- [13] Eissenberg JC, Elgin SC. The HP1 protein family: getting a grip on chromatin. *Curr Opin Genet Dev.* **2000**;10: 204–210.
- [14] Li Y, Kirschmann DA, Wallrath LL. Does heterochromatin protein 1 always follow code? *Proc Natl Acad Sci U S A.* **2002**;99(Suppl 4):16462–16469.
- [15] Bannister AJ, Zegerman P, Partridge JF, et al. Selective recognition of methylated lysine 9 on histone H3 by the HP1 chromo domain. *Nature.* **2001**;410:120–124.
- [16] Jacobs SA, Khorasanizadeh S. Structure of HP1 chromodomain bound to a lysine 9-methylated histone H3 tail. *Science.* **2002**;295:2080–2083.
- [17] Nakayama J, Rice JC, Strahl BD, et al. Role of histone H3 lysine 9 methylation in epigenetic control of heterochromatin assembly. *Science.* **2001**;292:110–113.
- [18] Lavigne M, Eskeland R, Azebi S, et al. Interaction of HP1 and Brg1/Brm with the globular domain of histone H3 is required for HP1-mediated repression. *PLoS Genet.* **2009**;5:e1000769.
- [19] Nielsen AL, Oulad-Abdelghani M, Ortiz JA, et al. Heterochromatin formation in mammalian cells: interaction between histones and HP1 proteins. *Mol Cell.* **2001**;7:729–739.
- [20] Larson AG, Elnatan D, Keenen MM, et al. Liquid droplet formation by HP1alpha suggests a role for phase separation in heterochromatin. *Nature.* **2017**;547:236–240.
- [21] Sanulli S, Trnka MJ, Dharmarajan V, et al. HP1 reshapes nucleosome core to promote phase separation of heterochromatin. *Nature.* **2019**;575:390–394.
- [22] Strom AR, Emelyanov AV, Mir M, et al. Phase separation drives heterochromatin domain formation. *Nature.* **2017**;547:241–245.
- [23] Erdel F, Rippe K. Formation of chromatin subcompartments by phase separation. *Biophys J.* **2018**;114: 2262–2270.
- [24] Erdel F, Rademacher A, Vlijm R, et al. Mouse heterochromatin adopts digital compaction states without showing hallmarks of HP1-driven liquid-liquid phase separation. *Mol Cell.* **2020**;78:236–249 e237.
- [25] Brero A, Easwaran HP, Nowak D, et al. Methyl CpG-binding proteins induce large-scale chromatin reorganization during terminal differentiation. *J Cell Biol.* **2005**;169:733–743.
- [26] Bertulat B, De Bonis ML, Della Ragione F, et al. MeCP2 dependent heterochromatin reorganization during neural differentiation of a novel Mecp2-deficient embryonic stem cell reporter line. *PLoS One.* **2012**;7:e47848.
- [27] Bosch-Presegue L, Raurell-Vila H, Thackray JK, et al. Mammalian HP1 isoforms have specific roles in heterochromatin structure and organization. *Cell Rep.* **2017**;21:2048–2057.
- [28] Raurell-Vila H, Bosch-Presegue L, Gonzalez J, et al. An HP1 isoform-specific feedback mechanism regulates Suv39h1 activity under stress conditions. *Epigenetics.* **2017**;12:166–175.
- [29] Hiragami-Hamada K, Soeroes S, Nikolov M, et al. Dynamic and flexible H3K9me3 bridging via HP1beta dimerization establishes a plastic state of condensed chromatin. *Nat Commun.* **2016**;7:11310.
- [30] Wongtawan T, Taylor JE, Lawson KA, et al. Histone H4K20me3 and HP1alpha are late heterochromatin markers in development, but present in undifferentiated embryonic stem cells. *J Cell Sci.* **2011**;124:1878–1890.
- [31] Mulholland CB, Smets M, Schmidtman E, et al. A modular open platform for systematic functional studies under physiological conditions. *Nucleic Acids Res.* **2015**;43:e112.
- [32] Gibson BA, Doolittle LK, Schneider MWG, et al. Organization of chromatin by intrinsic and regulated phase separation. *Cell.* **2019**;179:470–484 e421.
- [33] Shechter D, Dormann HL, Allis CD, et al. Extraction, purification and analysis of histones. *Nat Protoc.* **2007**;2:1445–1457.
- [34] Shakya A, Park S, Rana N, et al. Liquid-liquid phase separation of histone proteins in cells: role in chromatin organization. *Biophys J.* **2020**;118:753–764.
- [35] Turner AL, Watson M, Wilkins OG, et al. Highly disordered histone H1-DNA model complexes and their condensates. *Proc Natl Acad Sci U S A.* **2018**;115:11964–11969.
- [36] Muller-Ott K, Erdel F, Matveeva A, et al. Specificity, propagation, and memory of pericentric heterochromatin. *Mol Syst Biol.* **2014**;10:746.
- [37] Muller KP, Erdel F, Caudron-Herger M, et al. Multiscale analysis of dynamics and interactions of heterochromatin protein 1 by fluorescence fluctuation microscopy. *Biophys J.* **2009**;97:2876–2885.
- [38] Wang L, Gao Y, Zheng X, et al. Histone modifications regulate chromatin compartmentalization by contributing to a phase separation mechanism. *Mol Cell.* **2019**;76:646–659 e646.
- [39] Canzio D, Liao M, Naber N, et al. A conformational switch in HP1 releases auto-inhibition to drive heterochromatin assembly. *Nature.* **2013**;496:377–381.

- [40] Eberhart A, Feodorova Y, Song C, et al. Epigenetics of eu- and heterochromatin in inverted and conventional nuclei from mouse retina. *Chromosome Res.* 2013; 21:535–554.
- [41] Machida S, Takizawa Y, Ishimaru M, et al. Structural basis of heterochromatin formation by human HP1. *Mol Cell.* 2018;69:385–397 e388.
- [42] Maison C, Bailly D, Roche D, et al. SUMOylation promotes de novo targeting of HP1alpha to pericentric heterochromatin. *Nat Genet.* 2011;43:220–227.
- [43] Probst AV, Okamoto I, Casanova M, et al. A strand-specific burst in transcription of pericentric satellites is required for chromocenter formation and early mouse development. *Dev Cell.* 2010;19:625–638.